Fundamental characterisation of hemisphere free bulging using superplastic 8090 Al–Li sheets

T.-R. Chen, J. C. Huang, and Y. M. Hwang

Hemisphere free bulging of a superplastic 8090 Al–Li sheet was carried out, with particular emphasis given to the superplastic behaviour over the low strain regime $\varepsilon = 0$–$0{\cdot}7$. Various pressurising cycles, including constant pressure, constant strain rate, and multiple strain rate bulging, were performed to characterise the superplastic behaviour in terms of strain rate variation, thickness distribution, and evaluation of the strain rate sensitivity (m) of the sheet during biaxial bulging. For constant strain rate bulging, a modified Ghosh and Hamilton (GH) model and a model developed by the present authors (HL) have been used to simulate the necessary pressure profiles. Two different constitutive equations, extracted from uniaxial tensile tests, were used in the study. The modified GH model applied $\sigma = K\dot{\varepsilon}^m$ as the constitutive equation, i.e. considering only the m value in the simulation, while the HL model incorporated the strain hardening exponent (n) additionally into the constitutive equation for the simulation: i.e. the equation $\sigma = K'\varepsilon^n\dot{\varepsilon}^m$ was used. The HL model can also be applied to simulate the multiple stage strain rate forming route. Based on the analyses, the material superplasticity characteristics obtained from uniaxial tensile tests were seen to be reliably applicable to equibiaxial sheet bulging. The equibiaxial straining condition was not obeyed exactly except at the pole. With the consideration of initial work hardening contribution towards the constitutive equation, the simulated results seemed to agree better with the experimental data. With further straining, the rate sensitivity increased and work hardening decreased, thereby a multiple strain rate bulging path, including a high initial rate followed by several lower strain rates, would be able to fully utilise the higher values of m and n during each straining stage. The thickness uniformity as well as the total forming time could thus be improved and shortened. *MST/3107*

 Manuscript received 15 July 1994; in final form 4 May 1995. *Mr Chen and Professor Huang are in the Institute of Materials Science and Engineering, National Sun Yat-Sen University and Professor Hwang is in the Institute of Mechanical Engineering, National Sun Yat-Sen University, Kaohsiung, Taiwan.*

Introduction

A number of superplastic aluminium alloys have been successfully developed. These include the Al–Cu series (e.g. Supral 100 and 150), the Al–Mg series (e.g. 5083), the Al–Zn–Mg series (e.g. 7075 and 7475), and the Al–Li series (e.g. 2090 and 8090). Among these alloys, the Al–Li alloys have been recognised as attractive candidates for aircraft structure applications and their outstanding superplastic behaviour makes them especially competitive. Although the 8090 and 2090 Al–Li alloys exhibited uniaxial superplastic elongation in excess of 1000%,[1,2] the strain rate sensitivity $m = \mathrm{d}\ln\sigma/\mathrm{d}\ln\dot{\varepsilon}$ (one of the important parameters for superplasticity) at their optimum strain rate deformed to typical strain levels ($\varepsilon < 1{\cdot}4$) for superplastic forming (SPF) practices usually lies in the range 0·35–0·5 (Refs. 3–5) compared with ~0·75 (Refs. 6, 7) seen in the 7475 alloy. The lower value of m in the Al–Li alloys might suggest a less uniform strain distribution during SPF, which will be of great concern in practice and is worth further careful study. A fundamental understanding of the relationship between material characteristics and SPF strain distribution might be useful for finding optimum forming routes.

In order to simulate mathematically the optimum pressure profile for gas blowing SPF, numerous constitutive equations have been proposed to characterise the material flow stress response. A simple equation such as $\sigma = K\dot{\varepsilon}^m$ has been widely used, ignoring the work hardening since the material will be formed at high temperatures where the strain hardening for most cases is negligible. However, as was pointed out by, for example, Hamilton[8] or Chandra and Kannan,[9] the flow stress should be better expressed by $\sigma = K'\varepsilon^n\dot{\varepsilon}^m$ or $\sigma = K''\varepsilon^n\dot{\varepsilon}^m d^p$, where n ($= \mathrm{d}\ln\sigma/\mathrm{d}\ln\varepsilon$) is the work hardening exponent, d is the grain size, and p is a parameter to characterise grain growth during SPF and is usually around 2 for aluminium base alloys.[10] Since the highly superplastic Al–Li alloys are of the dynamically recrystallised type, the flow stress during the initial stage tends to reflect a higher work hardening rate; during this stage the microstructure transforms into fine grains with higher intergrain misorientation through dynamic recrystallisation.

Although the above argument has previously been considered, detailed experimental characterisation for this early stage of SPF in dynamically recrystallised materials has rarely been seen. It was the intention of the present study to conduct a fundamental characterisation for the forming behaviour of 8090 Al–Li alloy during hemisphere free bulging. The maximum average strain was limited to below 0·7: i.e. a very early stage for conventional superplastic forming practices.

Experimental procedures

The material used for superplastic forming was in the form of 1·65 mm thick 8090 SPF sheet, manufactured by Alcan and purchased from the Superform Company. The chemical composition of the sheet (wt-%) was Al–2·4Li–1·3Cu–0·63Mg–0·11Zr and the average grain/subgrain size in the as received sheet was ~4·5 μm. Specimens with a 10 mm gauge length were machined from the sheet with the tensile axis parallel to the rolling direction. The configuration of the tensile specimens is shown in Fig. 1. High temperature tensile tests were performed using a screw driven Instron 1125 universal

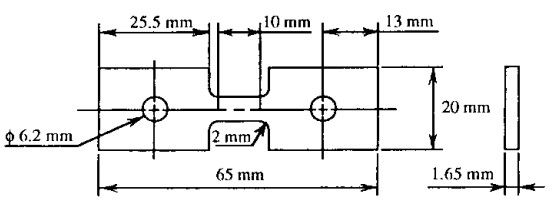

1 Specimen configuration for superplastic uniaxial tensile tests

testing machine, equipped with a three zone furnace in which a continuous stream of argon gas was flowing. Details of the tensile testing procedure have been given elsewhere.[11,12] The superplastic tensile tests were conducted at 510, 525, and 540 ± 1°C using strain rates in the range 10^{-5}–10^{-3} s^{-1}. An assumption of constant volume and uniform cross-sectional area over the gauge length was made in obtaining the stress–strain curves. This assumption was verified by stopping the test at $\varepsilon \sim 0{\cdot}5$, 1·0, and 1·5, and measuring the minimum cross-sectional area. It has been found that the discrepancy in using the assumption was sufficiently small (especially for $\varepsilon \leqslant 1{\cdot}0$), since the gauge section of the 8090 SPF sheet deformed sufficiently uniformly within this regime. To determine the strain rate sensitivity parameter m strain rate change tests were conducted. The basal strain rate basically remained a constant strain rate throughout the test. The strain rate difference between the basic and the enhanced rate was small (it increased by a multiplication factor of 0·25 to 2) and the elevated strain rate was maintained for a short period (equivalent to 0·03–0·05 true strain).[12] Hence, the microstructural difference resulting from the enhanced strain rate level could be assumed to be negligible.

The 8090 SPF sheet had been turned by a turning machine to produce specimens with a 95 mm diameter for the hemisphere free bulging tests. Before forming ~10 μm was ground off both sides of the specimen surface with an abrasive paper of 320 grit to remove the surface scratches, dirt, and grease from machining. The specimens were superplastically formed by using purpose designed apparatus[13] as shown in Fig. 2. The setup included both upper and lower parts, each of which had separate temperature and pressure control. Specimens for forming tests were placed on the top of the forming die, between the upper and lower sections. The cylindrical forming die had an inner diameter D of 60 mm, with two concentric raised clamping rings (with a diameter of 80 and 88 mm, respectively) of 0·4 mm height all around the die flange. The clamping force was provided by fastening the bolts connecting the upper and lower sections. The raised clamping rings would be forced into the specimen and stopped the part of the specimen in the flange portion (i.e. specimen materials outside the diameter of 80 mm) from pulling into the die during forming.

Both sections of the forming apparatus were equipped with a pressure transducer and solenoid valves to build up the necessary forming pressure during the tests. The forming pressure was closed loop monitored using an IBM PC, through controlling the solenoid valves according to simulated pressure profiles originally stored in a computer. Two different dies were used for the forming tests; the die entry radii were 3 and 8 mm respectively. Both dies were made of 4340 steel. Boron nitride was used as the lubricant between the die entry and the specimen to promote material sliding in this contact area. Argon gas was used for both pressurisation and for maintaining a protective atmosphere during SPF. The forming temperature was chosen to be 525 ± 3°C.

Hemispherical free bulging in a cylindrical open die was first performed under a constant forming pressure, partly for simplicity and partly for comparison with various theories. A pressure level of 345 kPa (i.e. 50 lb in^{-2}) was applied during most of the free bulging. It usually took approximately 5 min for the input pressure to reach the pressure level intended: i.e. a pressure increase rate of around 69 kPa min^{-1} (10 lb in^{-2} min^{-1}). Free bulging under a constant strain rate at $\sim 2 \times 10^{-4}$ s^{-1} was also conducted using the pressure profiles predicted by (a) a program[14] due to Ghosh and Hamilton (GH) which was originally written for long rectangular dies in the plane strain condition and has been modified in the authors' laboratory for hemisphere forming; and (b) a program[15]

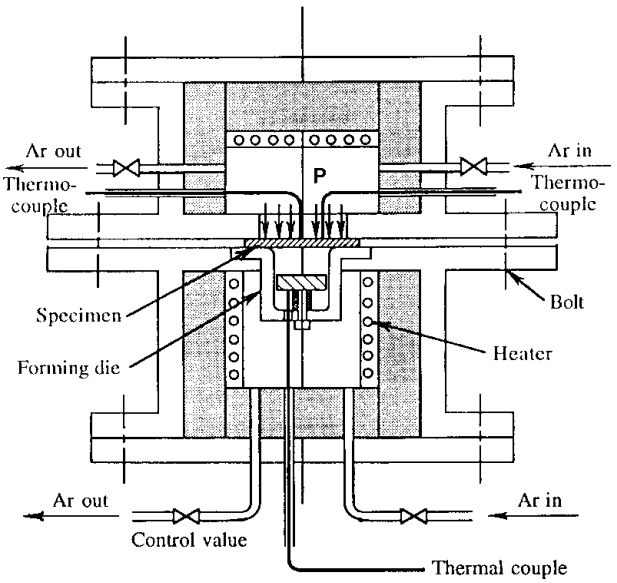

2 Schematic illustration of apparatus for superplastic forming

due to Hwang and Liauo (HL) which was selfwritten using the finite difference method. Basically, the modified GH model applied $\sigma = K\dot{\varepsilon}^m$ as the constitutive equation: i.e. considering only the strain rate sensitivity m for the flow stress in the simulation. The HL model incorporated the strain hardening exponent n additionally into the constitutive equation for the simulation: i.e. the equation $\sigma = K'\varepsilon^n\dot{\varepsilon}^m$ was used. In addition, the effects of various friction coefficients and die entry radii were also considered by the HL model.

The von Mises yield criterion was used by both models. Uniform thinning of the specimen thickness was assumed by both models for the free portion of the specimen during forming. The HL program can also be used to predict the resulting strain rate as a function of forming time under constant pressure conditions, as well as the thickness distribution of the formed samples. Meanwhile, in order to examine the effect of bulging pressure and thus the effective strain rate, several other bulging paths have been tried, including a higher constant pressure (e.g. 690 kPa or 100 lb in^{-2}), a more rapid pressure increase (e.g. 414 kPa min^{-1} or 60 lb in^{-2} min^{-1}), and multiple bulging stages with different strain rates.

Experimental results

CHARACTERISATION OF UNIAXIAL SUPERPLASTIC PROPERTIES

Table 1 gives the effects of test temperature and strain rate on the tensile superplastic elongation of the experimental 8090 Al–Li sheets. According to this table, the highest superplastic elongation occurred at 525°C for a strain rate of 2×10^{-4} s^{-1} where there was a constant strain rate condition. Furthermore, the superplastic elongation could be improved by a change to a constant crosshead speed (or decreasing strain rate) condition, and the highest elongation occurred at an initial strain rate of 8×10^{-4} s^{-1} at 525°C. Figure 3*a* shows the true stress–true strain curves for various strain rates at 525°C. Figure 3*b* and *c* shows the effect of the variation of m and n. An enlarged view of the variation of the value of m at low strains is shown in Fig. 3*d*. The relationship between the flow stress σ (in MN m^{-2}) and strain rate $\dot{\varepsilon}$ for this material strained at 525°C can be approximately expressed at

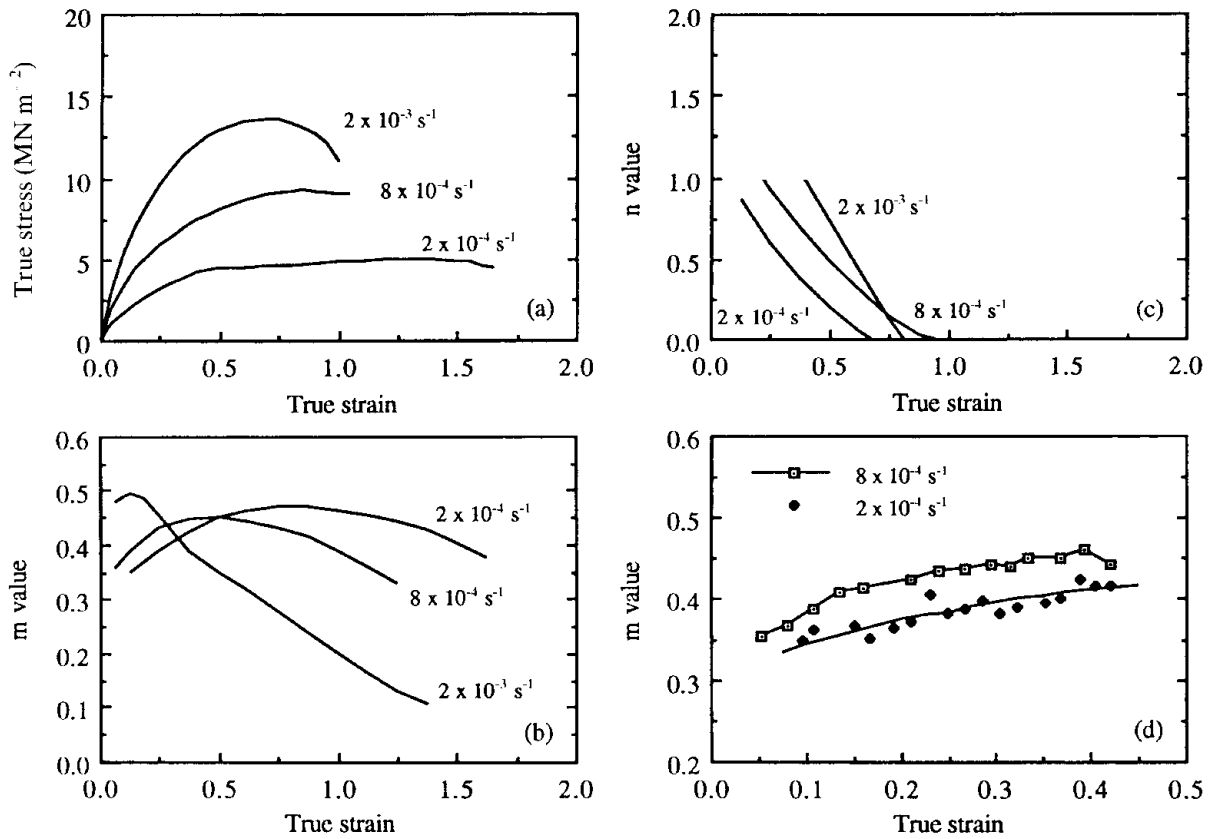

a true stress–true strain curves; *b* value of *m* at varying strain rates; *c* value of *n* at varying strain rates; *d* magnified version of *b* at low strain rate

3 Characteristics of experimental 8090 alloy

$\dot{\varepsilon} = 2 \times 10^{-4}\ s^{-1}$ by

$$\sigma = 268\varepsilon^{0.48} \quad (1a)$$

or at $\dot{\varepsilon} = 8 \times 10^{-4}\ s^{-1}$ by

$$\sigma = 233\varepsilon^{0.45} \quad (1b)$$

over the range $\varepsilon = 0.7$–1.5, where the work hardening contribution could be ignored. The flow stress at 2×10^{-4} or $8 \times 10^{-4}\ s^{-1}$, calculated by equation (1), is 4·5 or 9·0 MN m^{-2} respectively. For the initial stage of forming where the work hardening effect is more significant, another expression may be used

$$\sigma = K'\varepsilon^{n}\dot{\varepsilon}^{m} \quad (2)$$

which is applicable for $\varepsilon = 0.1$–0.7. The values of n were seen to vary from 1 to 0·35 and m from 0·3 to 0·48 over this strain range. The constant K' varies in accordance with the values of n and m. The grain growth effect was not considered in this study, thus no d^{p} term is included.

Table 1 Effects of test temperature and strain rate of uniaxial tensile tests on superplastic elongation of 8090 alloy

Test method	Test temperature, °C	Strain rate, s^{-1}	Elongation, %
Constant strain rate	540	2×10^{-3}	360
		8×10^{-4}	320
		2×10^{-4}	300
	525	2×10^{-3}	250
		8×10^{-4}	340
		2×10^{-4}	400
	510	2×10^{-3}	220
		8×10^{-4}	300
		2×10^{-4}	350
Constant crosshead speed	525	2×10^{-3} (initial)	350
		8×10^{-4} (initial)	550
		2×10^{-4} (initial)	470

From Fig. 3*a* and equation (2) it can be seen that the flow stress at $2 \times 10^{-4}\ s^{-1}$ in the strain interval $\varepsilon = 0.1$–0.7 varies from 1 to 4 MN m^{-2} or from 20 to 90% of the flow stress calculated from equation (1a). The lower flow stress of the material during this initial stage will undoubtedly result in a high forming rate for $\varepsilon = 0$–0.7. Meanwhile, the lower value of m and the higher value of n in the initial stage of forming will have opposing effects on the thickness uniformity as discussed by Ren *et al.*[4]

FREE BULGING IN CIRCULAR OPEN DIE

Constant pressure bulging

For simplicity, hemisphere free bulging was first conducted under constant pressure conditions. The results can easily be compared with a number of theories available. The forming temperature was chosen to be 525 ± 3°C in accordance with the results of the uniaxial tensile tests. Specimens blown from a die with an 8 mm die entry radius exhibited a higher bulge height h than those blown from a 3 mm one under the same forming conditions, as can be seen in Fig. 4*a*. The dependence of bulge height on the forming time tends to follow the theoretical predictions of Jovane[16] and Ragab.[17] The bulge heights of the specimens in both conditions showed a relatively high rate of increment at the beginning of bulging, then abruptly slowed down to a lower level, and increased again at longer forming times. The dependence of the ratio of the minimum thickness at the pole to the original sheet thickness s_p/s_0, maximum thickness-reduction strain ε_{max} at the pole, and maximum thickness strain rate at the pole $\dot{\varepsilon}_{max}$ as functions of the bulging time for both types of die are presented in Fig. 4*b*–*d*. The thickness strain rates at the pole when blowing with the 8 mm die always have a higher value, as shown in Fig. 4*d*, reflecting the higher strain rate which can be obtained from a larger die entry radius. It was also

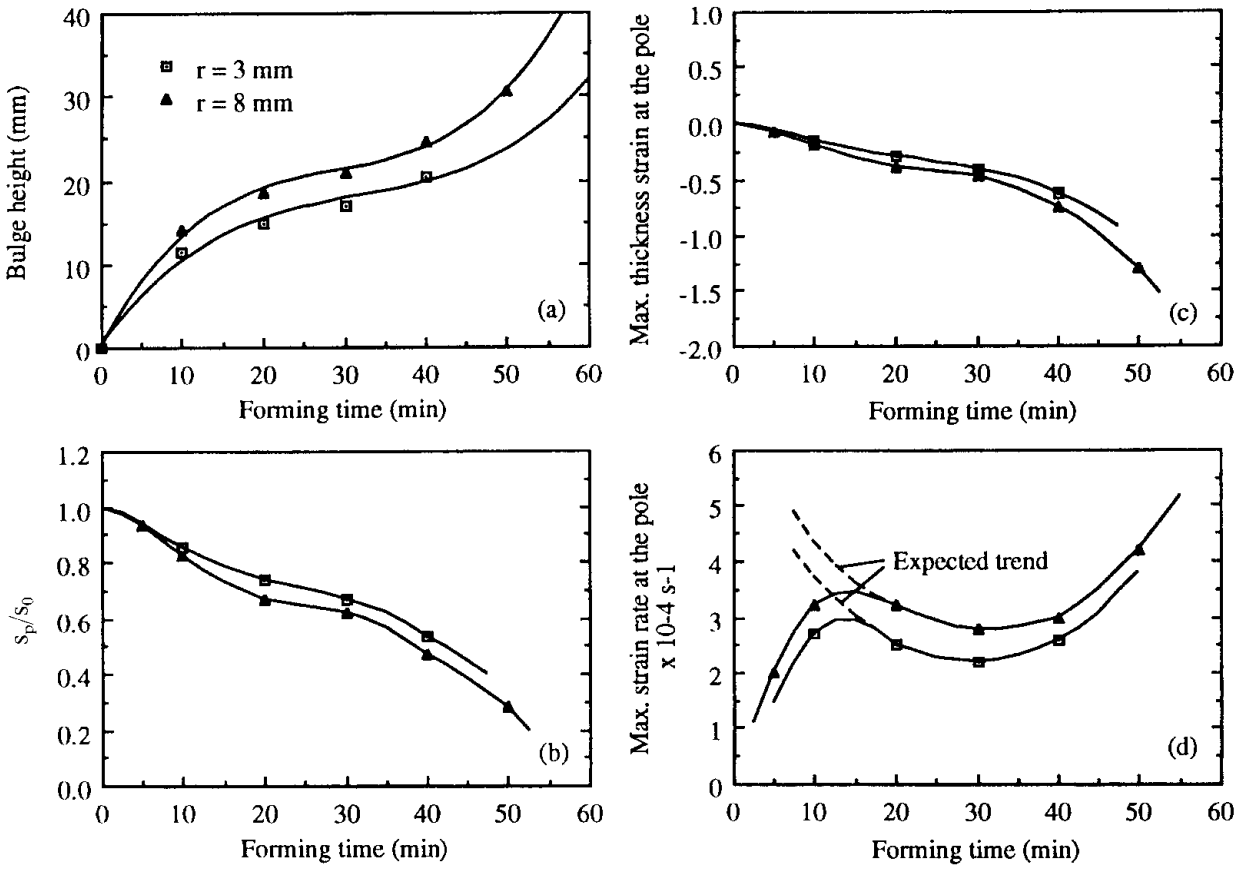

4 Dependence of *a* bulge height, *b* normalised minimum thickness at pole, *c* maximum thickness strain at pole, and *d* maximum thickness strain rate at pole as function of bulging time

noticed that the initial strain rate in Fig. 4*d* for $t < 15$ min was much lower than expected. The discrepancy was thought to be caused by the lower initial temperature due to the incoming cold argon gas. The temperature reading indicated a temperature drop of 20–30 K during this stage. The broken line in Fig. 4*d* is only a rough estimation for the case where the temperature is maintained constant from the onset of free bulging. A comparison of the experimentally observed strain rate values with the simulated predictions is presented in the Discussion section below.

The strain distributions in specimens blown by a constant forming pressure of 345 kPa (50 lb in^{-2}) in two different open dies for 10, 20, 30, and 40 min were measured and compared. Figure 5 gives the circumferential and meridional true strain distributions. The maximum circumferential and meridional strains were always found to be located at the pole, where the two strain components near the pole regime were seen to be the same: i.e. equibiaxial strain. At positions other than the pole, the meridional strain was higher than the circumferential strain, indicating the deviation from a perfect hemisphere. It can also be seen that the strain values in specimens blown from the 8 mm die were again consistently higher than in the case of the 3 mm one under the same bulging time.

Figure 6 shows the thickness distributions where the normalised thickness s/s_0 is used as a dimensionless parameter. Apparent localised thinning was found around the die entry for specimens blown from the die with a die entry radius of 3 mm (Fig. 6*a*). This was not observed when using the 8 mm die (Fig. 6*b*). The sharp die entry can induce a higher stress concentration in the specimen and suppress smooth metal flow, resulting in discontinuities in thickness distribution. This will also indirectly result in a lower bulge height increment rate (Fig. 4*a*) as well as a lower strain rate (Fig. 4*d*) in the 3 mm die.

In order to achieve a higher initial strain rate so as to take advantage of the higher values of m or n for $\varepsilon = 0$–$0{\cdot}25$ (Fig. 3*a*), the forming pressure as well as the initial rate of pressure increase were raised from 345 kPa (50 lb in^{-2}), 69 kPa min^{-1} (10 lb in^{-2} min^{-1}) to 690 kPa (100 lb in^{-2}), 414 kPa min^{-1} (60 lb in^{-2} min^{-1}), resulting in a higher initial strain rate from $\sim 3 \times 10^{-4}$ s^{-1} to $\sim 1 \times 10^{-3}$ s^{-1} respectively. The higher initial strain rate, accompanied by higher values of m and n, did improve the thickness distribution slightly, as seen in Fig. 7.

Constant strain rate bulging

Free bulging at constant strain rate was conducted primarily at 2×10^{-4} s^{-1}, using the pressure profiles simulated by the GH and HL models, as shown in Fig. 8. It will take approximately 70·5 and 39·6 min to blow a hemisphere (for a 0 and 8 mm die entry radius) according to the profiles simulated by the GH and HL models respectively. The friction coefficient used for simulating the pressure profile in Fig. 8 by the HL model was 0·3. Numerous pressure profiles for other bulging conditions have also been simulated by the HL model, including friction coefficients varying between 0 and ∞ (thus allowing partial or complete sliding along the die entry region), various die entry radii (0, 3, or 8 mm), and differing strain rates (2×10^{-4} s^{-1} to 2×10^{-3} s^{-1}). The influence of these factors on the resulting pressure profile is summarised in Table 2 in terms of the maximum and finishing pressure values (P_{max} and P_f) together with their corresponding times (t_{max} and t_f).

Experimentally, the true final bulge height for samples formed according to the pressure profiles shown in Fig. 8 was only 23 or 21 mm for the GH and HL case respectively, instead of the 30 mm expected for a hemisphere. This discrepancy might be partly due to the fact that both models can not account for the initial temperature drop

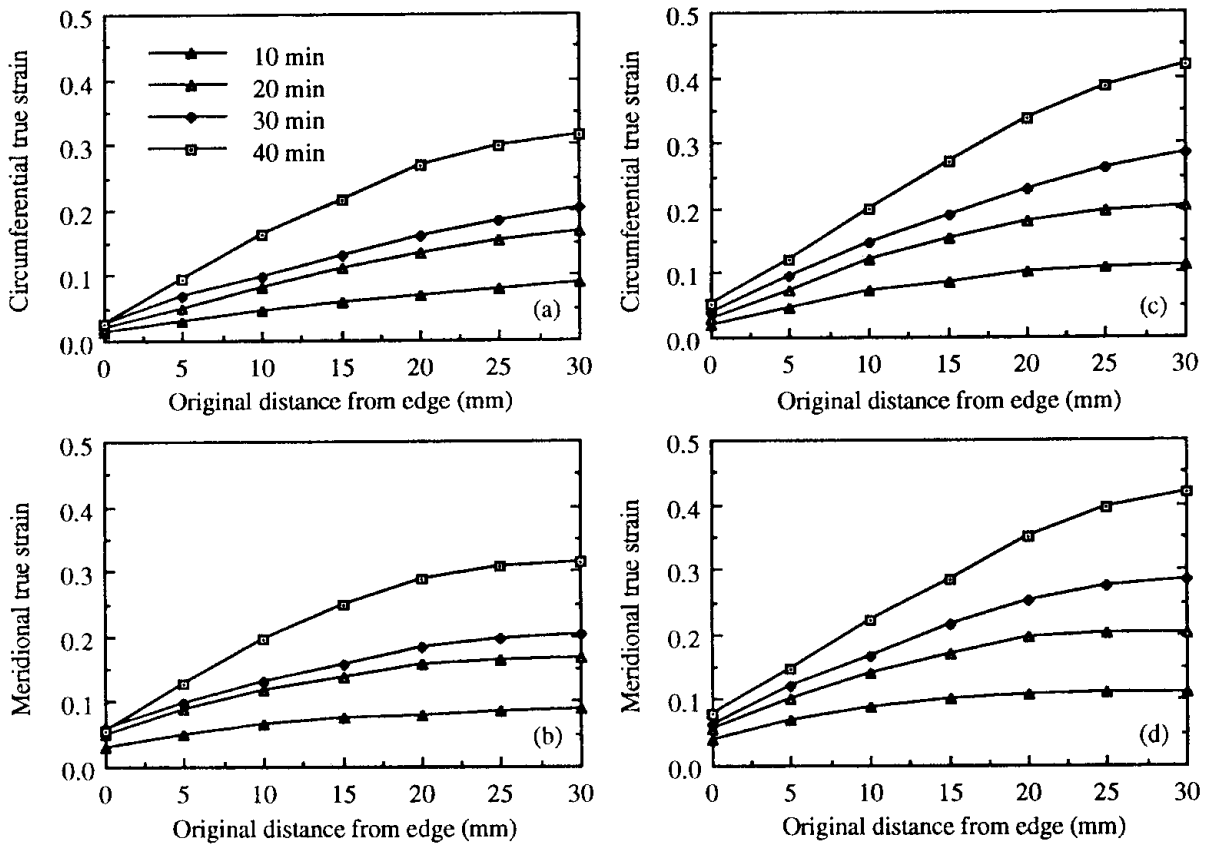

5 Strain distributions in 8090 specimens free bulged at 345 kPa with a rate of pressure increase of 69 kPa min^{-1} for various periods: *a* circumferential strains and *b* meridional strains in specimens bulged from 3 mm die entry radius; *c* circumferential strains and *d* meridional strains in specimens bulged from 8 mm die entry radius

caused by the incoming cold gas. In addition to this effect, the oversimplified assumptions might also result in pressure profiles lower than that actually required. The maximum pressure in their simulated profiles (Fig. 8) for $2 \times 10^{-4}\,s^{-1}$ was less than 311 kPa (45 lb in^{-2}) which is lower than the level (345 kPa or 50 lb in^{-2}) that was input for the case of constant pressure free bulging. The thickness distribution for the samples blown under constant strain rate is shown in Fig. 9. Since the actual maximum strain rate at the pole experimentally measured under the constant strain rate condition was around $1{\cdot}5 \times 10^{-4}\,s^{-1}$ (using the GH model) or $2{\cdot}2 \times 10^{-4}\,s^{-1}$ (using the HL model), which was only slightly lower than the measured strain rate under the constant pressure condition to equivalent bulging height ($\dot{\varepsilon}_{max} \sim 2{\cdot}8 \times 10^{-4}\,s^{-1}$), the thickness distribution profiles for the two constant strain rate cases were only slightly worse than the constant pressure ones (Fig. 9).

Table 2 Influence of friction coefficients μ_d, die entry radius r_e, and strain rate $\dot{\varepsilon}$ on resulting pressure profile in terms of the maximum pressure P_{max}, finishing pressure P_f, and their corresponding times t_{max} and t_f respectively: all of the data were simulated by the HL model

$\dot{\varepsilon}$, s^{-1}	μ_d	r_e, mm	P_{max}, KPa	P_f, KPa	t_{max}, min	t_f, min
2×10^{-4}	0	3	324	281	24·5	46·5
2×10^{-4}	0·3	3	320	273	25·9	48·2
2×10^{-4}	0·56	3	317	270	26·2	52·2
2×10^{-4}	∞	3	311	256	26·7	54·4
2×10^{-4}	0	8	318	305	26·0	37·4
2×10^{-4}	0·3	8	314	297	27·2	39·6
2×10^{-4}	0·56	8	311	292	28·0	41·1
2×10^{-4}	∞	8	295	266	29·4	48·7
2×10^{-4}	0·3	0	321	247	25·6	57·8
2×10^{-4}	0·3	3	320	273	25·9	48·2
2×10^{-4}	0·3	8	314	297	27·2	39·6
2×10^{-4}	∞	0	321	247	25·6	57·8
2×10^{-4}	∞	3	311	256	26·7	54·4
2×10^{-4}	∞	8	295	266	29·4	48·7
2×10^{-4}	0·3	8	314	297	27·2	39·6
5×10^{-4}	0·3	8	471	440	10·2	15·0
8×10^{-4}	0·3	8	611	577	6·8	9·9
2×10^{-3}	0·3	8	948	896	2·7	4·0

Variable strain rate bulging

In order to prevent localised thinning during forming, or necking during tensile loading, it is usually necessary to satisfy the criterion $d\sigma/d\varepsilon > \sigma$. By expanding $d\sigma/d\varepsilon$

$$d\sigma/d\varepsilon = (\partial\sigma/\partial\varepsilon) + (\partial\sigma/\partial\dot{\varepsilon})(d\dot{\varepsilon}/d\varepsilon)$$
$$= n(\sigma/\varepsilon) + m(\sigma/\dot{\varepsilon})(d\dot{\varepsilon}/d\varepsilon) \quad \ldots\ldots\ldots (3)$$

it can be seen that a combination of higher n and m values will help to satisfy $d\sigma/d\varepsilon > \sigma$, thus preventing localised thinning and promoting uniform thickness distribution. This effect has been partly observed in Fig. 7. Based on Fig. 3*b* and *c*, the optimum bulging path should involve continuously variable strain rates; during each period the combination of m and n should always be highest. Experimentally, a simple forming route may consist of multiple stages, each with a constant strain rate. For example, a bulging path with a high initial strain rate of $2 \times 10^{-3}\,s^{-1}$ for $\varepsilon = 0$–$0{\cdot}25$, followed by an intermediate rate of $8 \times 10^{-4}\,s^{-1}$ for $\varepsilon = 0{\cdot}25$–$0{\cdot}5$, and finishing with a lower strain rate of $2 \times 10^{-4}\,s^{-1}$ for $\varepsilon = 0{\cdot}5$–$0{\cdot}7$, will be able to fully utilise the higher m and n values during each straining stage. The pressure profile corresponding to such a bulging path, simulated by the HL model, is shown in Fig. 10*a*.

Theoretically, it will take only 8 min to complete a hemisphere with a bulging height of 30 mm (compared with the forming time of 39·6 min needed for the constant strain

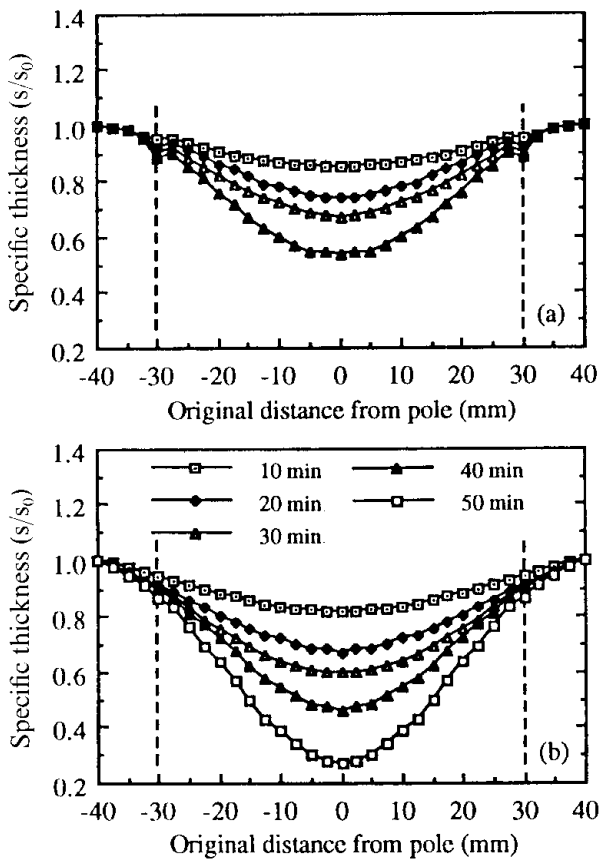

a 3 mm; *b* 8 mm

6 Thickness distribution of the specimens free bulged at 345 kPa with rate of increase of 69 kPa min^{-1} for various periods in circular open dies with given die entry radius: vertical broken lines refer to die edge (inner die diameter was 60 mm)

rate condition at 2×10^{-4} s^{-1}). In contrast, experimentally the finishing bulging height was 20 mm. This was again partly due to the initial lower temperature and partly due to the discrepancy between the theory and experiment. Figure 10*b* shows the thickness distribution, in comparison with those of the samples bulged under the constant pressure or constant strain rate condition. It is obvious that the thickness uniformity has been improved, consistent with the prediction. This effect was not only seen for open

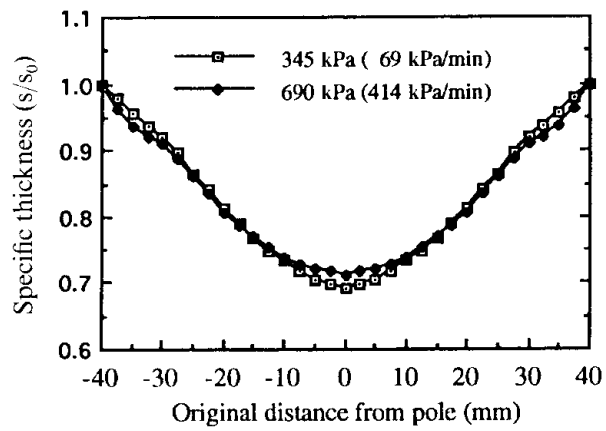

7 Comparison between thickness distributions in samples bulged with a forming pressure and rate of pressure increase of either 345 kPa and 69 kPa min^{-1} or 690 kPa and 414 kPa min^{-1}: bulge height for both samples was 18 mm

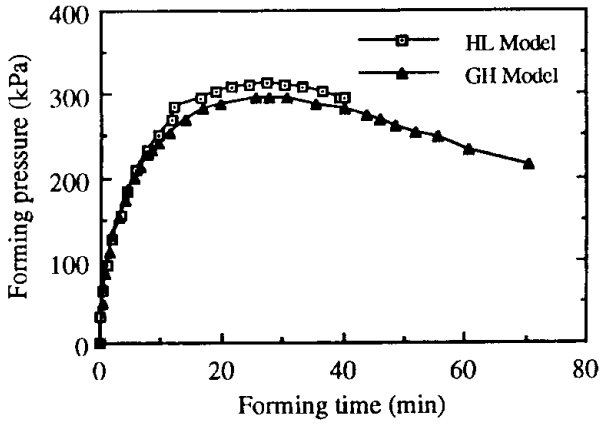

8 Comparison of forming profiles simulated by GH and HL models (effective strain rate = 2×10^{-4} s^{-1}): GH model assumes complete sticking ($\mu = \infty$) along die entry with die entry radius $r_e = 0$ mm, and the HL model for this profile assumes partial sliding with friction coefficient of 0·3 and $r_e = 8$ mm

die free bulging, the same improvement has also been observed for closed die forming. Figure 10*c* is an example for a circular pan with $h/D = 1/3$. The forming time was reduced from 80·2 to 10·2 min, in addition to obtaining an improved thickness distribution.

Discussion

FORMING STRAIN RATE DURING FREE BULGING

The measured maximum thickness strain rates at the pole of specimens free bulged with the die entry radii of 3 and 8 mm to different h/D ratios were seen to lie in the range $(2–4·5) \times 10^{-4}$ s^{-1}. An attempt has been made to evaluate the relationship between the input pressure and the resulting strain rate. It should be noted first that the total strain experienced during hemisphere free bulging is very small; the average strain was no greater than 0·7 and the maximum strain at the pole was no greater than 1·3. Bearing in mind the results in Fig. 3, one can not overlook the initial work hardening behaviour as well as the variable value of m during the early stage of straining: e.g. when considering hemisphere bulging equation (2), instead of equation (1), should be more applicable.

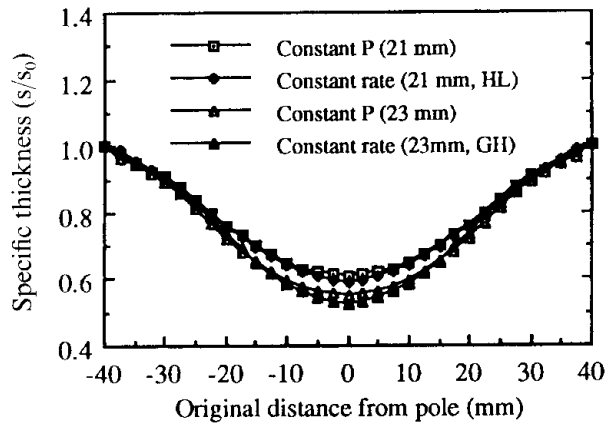

9 Comparison of thickness distribution for specimen bulged under constant pressure (345 kPa) and constant strain rate (2×10^{-4} s^{-1}) conditions using forming profiles simulated by GH and HL models: bulge height was either 21 or 23 mm

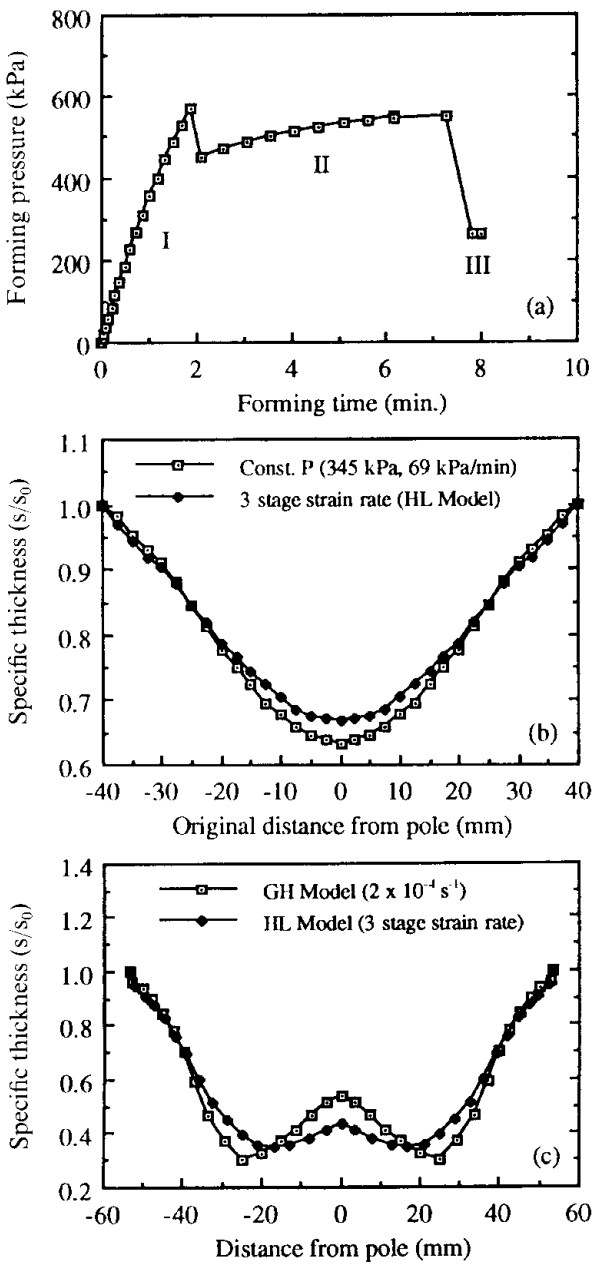

10 ***a*** **pressure profile corresponding to multiple strain rate bulging (stage I: $\dot{\varepsilon} = 2 \times 10^{-3}\ s^{-1}$ for $\varepsilon = 0$–0·25; stage II: $\dot{\varepsilon} = 8 \times 10^{-4}\ s^{-1}$ for $\varepsilon = 0{\cdot}25$–0·5; and stage III: $\dot{\varepsilon} = 2 \times 10^{-4}\ s^{-1}$ for $\varepsilon = 0{\cdot}5$–0·7) and** ***b*** **the resulting experimentally measured thickness distribution, as compared with the one bulged under constant pressure condition at 345 kPa: a similar effect was also applicable to forming with $h/D = 1/3$ shown in** ***c***

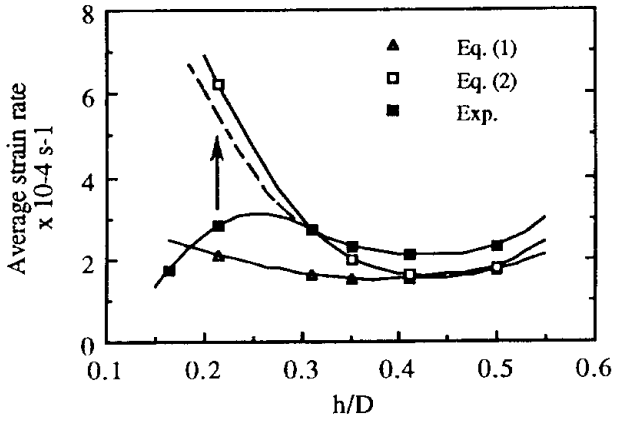

11 Variation of experimentally measured average strain rate of specimens free bulged using 8 mm die compared with predictions of equation (1) and equation (2) (Eq. (1) and Eq. (2)): broken line represents an extension of experimental data (Exp.) to low h/D values illustrating the case when no initial temperature drop involved

By fitting equation (2) using the data in Fig. 3, the values of K', n, and m can be determined for each range of strain level (e.g. 0–0·1, 0·1–0·2, etc.) at each strain rate. With the parameters determined in equation (2), the strain rate for various strain levels under constant pressure conditions can be calculated. Finally, the calculated strain rate should be corrected by considering (a) the flowing in effect from die entry and (b) the initial gradual pressure increase during the first 5 min of pressure input. The first factor should be considered since the outer materials can flow into the inner hemisphere via die entry which has a radius of 8 mm and was painted with boron nitride as lubricant. The second factor will be especially important during, for example, the first 10 min of forming. Both factors can be corrected by an internal computer program[15] with the capability to account for sliding according to the respective friction coefficients μ.

Table 3 summarises the calculated strain rate values assuming uniform thinning, which may be compared with the experimentally measured 'average' strain rates. The latter data can be easily determined in accordance with the experimental measured bulge height with the assumption of uniform thinning. The average strain rates obtained differ from and are lower than the measured maximum strain rate at the pole. It can be seen from Table 3 or Fig. 11 that the strain rate values calculated from equation (2) are generally in better agreement than those calculated from equation (1) except for the first 10 min of bulging where the actual temperature dropped below 525°C due to the rapid ingress of cold argon gas. It was difficult to take this initial temperature drop into account when simulating the strain rate values since the entire material parameters at $T = 480$–510°C and $\dot{\varepsilon} = 2 \times 10^{-4}$ to $2 \times 10^{-3}\ s^{-1}$ were still incomplete.

It was also found that the difference between strain rate values obtained by using equations (1) and (2) can be evaluated by the difference in flow stress of the materials tested by uniaxial tensile loading. A lower flow stress will result in a much higher strain rate, under the same condition of constant pressure during free bulging, as shown in Fig. 12. For $\varepsilon = 0{\cdot}1$–0·2, the ratio $\sigma_{Eq.(2)}/\sigma_{Eq.(1)} \approx 0{\cdot}3$, corresponding to a strain rate ratio of ~12. It is apparent that the forming rate for the early stage of hemisphere free bulging will be markedly different. However, the values of strain rates calculated from equation (2) in Table 3 were not seen to be so high, at least not as high as a factor of 12 higher than those calculated from equation (1).

Table 3 Comparison between theoretically predicted ($\dot{\varepsilon}_{Eq.(1)}$ and $\dot{\varepsilon}_{Eq.(2)}$) and experimentally measured $\dot{\varepsilon}_{Expt}$ values of strain rate under constant pressure (345 kPa/50 lb in^{-2}) free bulging

h/D	ε	$\dot{\varepsilon}_{Eq.(1)}$, $10^{-4}\ s^{-1}$	$\dot{\varepsilon}_{Eq.(2)}$, $10^{-4}\ s^{-1}$	$\dot{\varepsilon}_{Expt}$, $10^{-4}\ s^{-1}$
0·00–0·21	0·00–0·17	2·1	6·2	2.8*
0·21–0·30	0·17–0·32	1·6	2·7	2·7
0·30–0·34	0·32–0·41	1·5	2·0	2·3
0·34–0·40	0·41–0·50	1·5	1·6	2·1
0·40–0·50	0·50–0·70	1·7	1·8	2·3

* The measured data on average strain rate during this period was lower than expected since the temperature during this initial stage dropped due to the incoming cold argon gas.

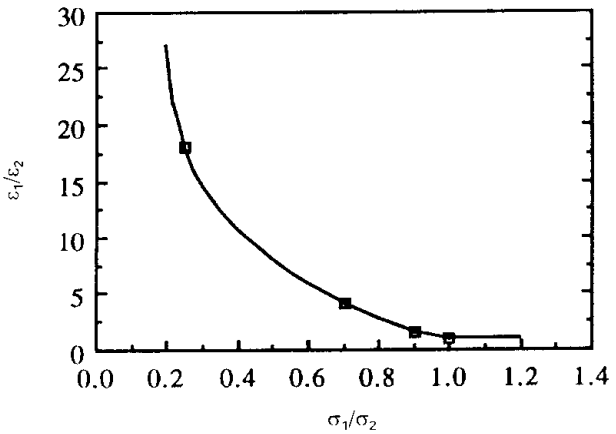

12 Plot of $\dot{\varepsilon}_1/\dot{\varepsilon}_2$ versus σ_1/σ_2 for 8090 alloy showing the effect of different flow stresses on the resulting strain rate under constant forming pressure condition

This is because once the sample was bulged at a higher strain rate during this initial stage, e.g. $\varepsilon = 0{\cdot}1$–$0{\cdot}2$, the actual material flow stress will also increase. For example, the flow stress at $2 \times 10^{-4}\,s^{-1}$ over $\varepsilon = 0{\cdot}1$–$0{\cdot}2$ was around 1·4 MN m^{-2} but the flow stress at 12 times $2 \times 10^{-4}\,s^{-1}$, i.e. $2{\cdot}4 \times 10^{-3}\,s^{-1}$, will be ~ 8 MN m^{-2}, but a high material flow stress will not allow the sample to bulge at $2{\cdot}4 \times 10^{-3}\,s^{-1}$. A reasonable strain rate will be one that matches the input pressure capability. In Table 3, it appears that a strain rate of $\sim 6 \times 10^{-4}\,s^{-1}$, at which the material flow stress is $\sim 4{\cdot}5$ MN m^{-2} is a reasonable value. The sample will always find its 'comfortable' strain rate, suitably reflecting the response to input pressure as well as to the material characteristics. The calculated strain rate values were extracted from this iterative method.

In addition, the current strain rate can also be compared with other theoretical analyses made by Jovane[16] and Cornfield and Johnson[18] for free bulging by constant pressure. The minimum strain rate, according to Jovane's theory, should occur at $h/D \sim 0{\cdot}3$, which is approximately the region observed in the current study ($h/D = 0{\cdot}35$–$0{\cdot}4$). Although the theory of Jovane did not consider the variation of thickness distribution, the effect of which is significant in the current case, the overall average strain rate extracted from this theory is still close to the measured strain rates. The current result implies that the net observed strain rate, considering both the thinner region at the pole and the thicker region near the die entry, can still be approximately estimated by the simple theory of Jovane.

It is worth mentioning that a constant pressure of 345 kPa (50 lb in^{-2}) corresponds to a variable strain rate (if the temperature remains constant), from $\sim 1 \times 10^{-3}\,s^{-1}$ initially, to the minimum strain rate of $\sim (2$–$3) \times 10^{-4}\,s^{-1}$, followed by a gradual increase to the final rate of $4 \times 10^{-4}\,s^{-1}$. The initial high strain rate (accompanied by a higher material flow stress) actually helps the partially recrystallised subgrains develop into well defined grains[19] which are suitable for grain boundary sliding. The subsequent lower strain rate at $(2$–$4) \times 10^{-4}\,s^{-1}$ will then be the optimum strain rate for superplastic forming. In other words, a constant pressure condition for hemisphere free bulging of partially recrystallised 8090 sheets is not only easier for industrial operation but is also a more favourable route than a constant strain rate condition.

CIRCUMFERENTIAL AND MERIDIONAL STRAIN VARIATION

As can be seen in Fig. 5, the maximum circumferential and meridional strains are located at the pole in all specimens. The circumferential and meridional strains were seen to be

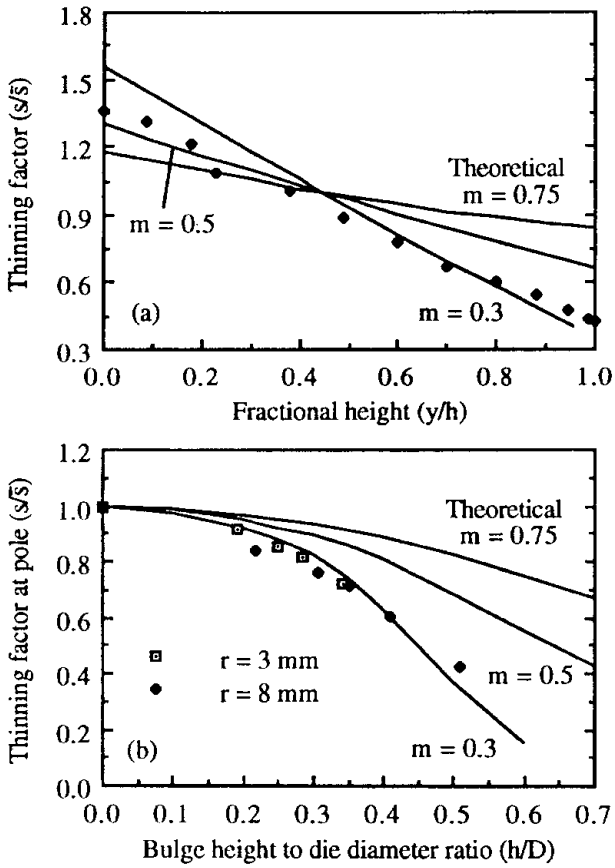

13 Comparison of *a* theoretical and experimental thinning factor for 8090 specimen free bulged to a hemisphere; and *b* theoretical and experimental thinning factor at pole of specimen free bulged from circular open die: solid lines represent theoretical predictions for given values of *m* after Cornfield and Johnson[18]

the same at the pole for every specimen free bulged from the circular open die, which implied that the condition for equibiaxial stress occurs at this point of specimen only. In the rest of the specimen, the meridional strain was found to be higher than the circumferential strain. It appears that the deformation of specimen in the meridional direction has less restriction than that in the circumferential direction. This is thought to be a result of preferred thinning around the pole, making an easier path for straining along the meridional direction. Eventually, the shape of the bulged piece will deviate from a hemisphere into a somewhat ellipsoidal shape. The tendency to form an ellipsoidal shape will be higher when the m value is low, as in the case discussed recently by Yang and Mukherjee.[20]

THICKNESS DISTRIBUTION

The thickness distribution can be seen to become more non-uniform as the bulging continues. The m value of 8090 alloy bulged in the current forming conditions can also be evaluated by comparing the experimental data directly to the theoretical thinning curves provided by Cornfield and Johnson,[18] as shown in Fig. 13*a*. The experimental data shown in this figure were selected from a specimen free bulged with the 8 mm entry radius. A thinning factor $s/\bar{s}$, defined by the ratio of the actual thickness to the average thickness,[18] was used in this figure. The average thickness is the one which would result if the material stretched in a completely uniform manner.

The value of m obtained from Fig. 13*a* was close to 0·3–0·4, consistent with the values obtained from uniaxial

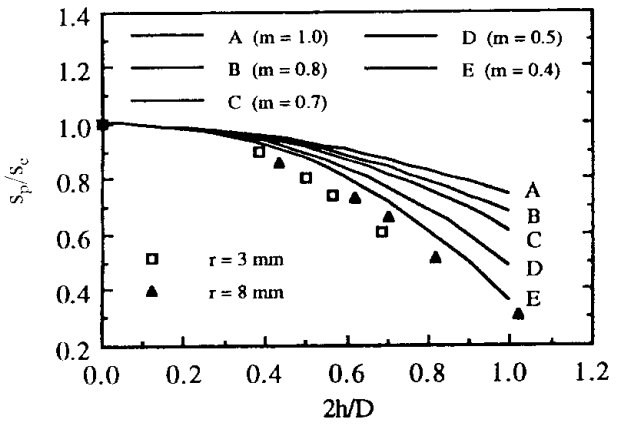

14 Comparison of theoretical and experimental thinning factor s_p/s_e at pole of 8090 specimen free bulged from circular open die: solid lines theoretical predictions for given values of m after Chandra and Kannan[21]

tensile tests for $\varepsilon = 0$–$0{\cdot}7$ (*see* Fig. 3*b* or *d*). Comparison of the experimental data with the theoretical thinning curves provided by Cornfield and Johnson[18] for the thinning factor at the pole for various h/D ratios again suggested a low m value of $\sim 0{\cdot}3$ (*see* Fig. 13*b*). Both the experimental data for specimens bulged from the 3 mm and 8 mm dies are included in the latter figure. The observed low value of m is also in agreement with the measured data in Fig. 3*b* or *d*. The value of strain rate sensitivity appeared to be low for the initial stage of straining (as in the case of hemisphere bulging), during which the work hardening contribution to the superplastic straining was appreciable. With further straining, the value of m increased and value of n decreased making the material flow finally completely controlled by the strain rate sensitivity.

Comparison of the experimental data to the theoretical thinning curves predicted by Chandra and Kannan[21] have also been made, as shown in Fig. 14. A thinning factor s_p/s_e, defined by the ratio of the thickness at the pole to the thickness at the edge,[21] was used in this figure. The experimental data for specimens bulged from dies with both 3 and 8 mm entry radii are included in this figure. As can be seen in the figure, the experimental data still suggested a low value of m of $\sim 0{\cdot}3$.

The above analysis and comparison for the simple shaped hemisphere bulging, in terms of strain rate variation, thickness distribution, and m value evaluation, suggests that the material superplasticity characteristics obtained from uniaxial tensile tests are indeed applicable to equibiaxial sheet bulging. Deviation from the spherical shape is not seen to be severe when hemisphere bulging is being considered, even when the m value is as low as 0·3. However, this is not true when the bulging is intended to proceed much further than a hemisphere: e.g. a deep cone or box.

Summary

The observations from the experimental results and data analyses are summarised below.

1. For hemisphere bulging, the inclusion of the initial work hardening contribution in the constitutive equations seemed to offer better simulated results.

2. Under the same forming conditions, a higher forming height can be achieved by using a die with a larger die entry radius. The thickness strains and strain rates at the pole when using an 8 mm die always have higher values than when using a 3 mm die under the same forming conditions, reflecting that a higher strain rate can result from a larger die entry radius.

3. The meridional strain was found to be slightly higher than the circumferential strain except at the pole of a hemisphere. This suggests that the equibiaxial straining condition was not completely obeyed except at the pole.

4. Specimens free bulged under constant pressure (initial decreasing strain rates) can result in a better thickness distribution than those formed via the constant strain rate route.

5. A multiple strain rate bulging path, including a high initial strain rate followed by an intermediate rate and finished by a lower strain rate, is able to fully utilise the higher m and n values during each straining stage. The thickness uniformity as well as the total forming time can be improved and shortened.

6. The m value appears to be rather low for the initial stage of straining (as in the case of hemisphere bulging), during which period the work hardening contribution to the superplastic straining was appreciable. With further straining, the m value increases and n value decreases making the material flow finally dominated by the strain rate sensitivity.

7. The experimental measured superplastic straining behaviour during free bulging was seen to be in reasonable agreement with various existing theories, including the strain rate variation as a function of pressure, strain distribution, and the m value dependence. The m values for this material for $\varepsilon = 0$–$0{\cdot}7$ obtained from direct measurements and theoretical analyses fell in the range 0·3–0·45.

Acknowledgements

The authors would like to thank Dr H.-P. Pu for immeasurable help in preparing this paper. The sponsorship from the Aero Industries Development Center, Taichung, Taiwan and the Metal Industries Development Center, Kaohsiung, Taiwan is gratefully acknowledged. The authors also thank Professor N. Chandra and Professor A. K. Ghosh for their helpful comments.

References

1. W. S. MILLER and J. WHITE: in 'Superplasticity in aerospace', (ed. H. C. Heikkenen and T. R. McNelley), 211–228; 1988, Warrendale, PA, AIME.
2. J. WADSWORTH, A. R. PELTON, and R. E. LEWIS: *Metall. Trans. A*, 1985, **16A**, 2319–2332.
3. T. J. WATSON and J. I. BENNETCH: in 'Superplasticity in aerospace', (ed. H. C. Heikkenen and T. R. McNelley), 261–297; 1988, Warrendale, PA, AIME.
4. B. REN, C. H. HAMILTON, and B. ASH: in 'Aluminium–lithium alloys V', (ed. T. H. Sanders and E. A. Starke), 131–139; 1989, Birmingham, MCEP.
5. A. S. D'OLIVEIRA, P. S. BATE, and W. T. ROBERTS: in 'Processing, properties and applications of metallic and ceramic materials', (ed. M. H. Loretto and C. J. Beevers), 1001–1006; 1992, Birmingham, Industrial Research Centre.
6. N. E. PATON, C. H. HAMILTON, J. A. WERT, and M. W. MAHONEY: *J. Met.*, 1982, **34**, (8), 21–27.
7. A. K. GHOSH and C. H. HAMILTON: *Metall. Trans. A*, 1982, **13A**, 733–743.
8. C. H. HAMILTON: in 'Formability analysis, modeling and experimentation', (ed. S. S. Hecker, *et al.*), 232; 1978, Warrendale, PA, AIME.
9. N. CHANDRA and D. KANNAN: *J. Mater. Eng. Perform.*, 1992, **1**, 801–812.
10. A. ARIELI and A. K. MUKHERJEE: *Metall. Trans. A*, 1982, **13A**, 717–732.

11. H.-P. PU, S.-H. YEN, J. C. HUANG, and P.-W. KAO: in Proc. ICSAM–91, Osaka, Japan, The Japan Society for Research on Superplasticity, 429.
12. H.-P. PU, F. C. LIU, and J. C. HUANG: *Metall. Mater. Trans. A*, 1995, **26A**, 1153–1166.
13. T.-R. CHEN and J. C. HUANG: *Chin. J. Mater. Sci.*, 1993, **25**, 34–49.
14. A. K. GHOSH and C. H. HAMILTON: in 'Process modeling fundamentals and applications to metals', (ed. T. Altan *et al.*), 303; 1980, Metals Park, OH, ASM.
15. Y. M. HWANG, J. M. LIEW, T. R. CHEN, and J. C. HUANG: *J. Mater. Process. Technol.*, 1996, **57**, 360–372.
16. F. JOVANE: *Int. J. Mech. Sci.*, 1968, **10**, 403–427.
17. A. R. RAGAB: *Met. Technol.*, 1983, **10**, 340–348.
18. G. C. CORNFIELD and R. H. JOHNSON: *Int. J. Mech. Sci.*, 1970, **12**, 479–490.
19. N. RIDLEY: *Mater. Sci. Technol.*, 1990, **6**, 1145–1156.
20. H. S. YANG and A. K. MUKHERJEE: *Int. J. Mech. Sci.*, 1992, **34**, 283–297.
21. N. CHANDRA and D. KANNAN: *J. Mater. Eng. Perform.*, 1992, **1**, 813–822.